Accuracy and Precision of Compartmental Model Parameters Obtained from Directly Estimated Dynamic SPECT Time-Activity Curves

Bryan W. Reutter, *Member, IEEE,* Grant T. Gullberg, *Fellow, IEEE,* and Ronald H. Huesman, *Fellow, IEEE*

***Abstract*— Quantitative kinetic analysis of dynamic cardiac single photon emission computed tomography (SPECT) data has the potential to provide better contrast between healthy and diseased tissue, compared to static images. However, imaging a rapidly changing radiopharmaceutical distribution with the use of a moving gantry yields inconsistent projection data that can generate artifacts in a time sequence of conventional image reconstructions. The artifacts can lead to biases in kinetic parameters estimated from the image sequence. This source of bias can be eliminated by estimating B-spline models for time-activity curves directly from the projections. In this study, we perform Monte Carlo simulations to determine how the polynomial order and initial time sampling of the splines affect the accuracy and precision of compartmental model parameters obtained from directly estimated time-activity curves. The Mathematical Cardiac Torso (MCAT) phantom is used to simulate a realistic 15 min dynamic ^{99m}Tc-teboroxime patient study in which 10 million total events are detected. For a large volume of normal myocardium (250 cc), the relative bias of the uptake and washout parameter sample means does not exceed 0.3% when using cubic or quadratic splines that provide rapid initial sampling. The coefficient of variation is about 1%. For small (8.4 cc) myocardial defects that exhibit reduced uptake and accelerated washout, the relative bias and coefficient of variation increase to maximum values of about 16% and 50%, respectively. These levels of accuracy and precision provide good contrast between the compartmental model time-activity curves for the defects and normal myocardium. There is also good contrast for compartmental model time-activity curves obtained from noisy data containing 5 million events.**

***Index Terms*— dynamic single photon emission computed tomography (SPECT), fully four-dimensional (4-D) reconstruction, kinetic parameter estimation**

I. Introduction

QUANTITATIVE kinetic analysis of dynamic cardiac single photon emission computed tomography (SPECT) data has the potential to provide better contrast between healthy and diseased tissue, compared to static images [1]. However, imaging a rapidly changing radiopharmaceutical distribution with the use of a moving gantry yields inconsistent projection data that can generate artifacts in a time sequence of conventional image reconstructions. The artifacts can lead to biases in kinetic parameters estimated from time-activity curves obtained by overlaying volumes of interest on the image sequence. This source of bias can be eliminated by faithfully modeling the time variation of the activity distribution throughout the projected field of view and estimating temporal model parameters directly from the projection data [2]–[11].

Previously, we used temporal B-spline basis functions to model time courses of activity within segmented volumes and developed fast methods to estimate spline model coefficients and their statistical uncertainties directly from dynamic SPECT projection data [6], [10]. In the present work, we perform Monte Carlo simulations of realistic dynamic cardiac ^{99m}Tc-teboroxime patient studies to determine how the polynomial order and initial time sampling of the splines affect the accuracy and precision of compartmental model parameters obtained from directly estimated time-activity curves. It is anticipated that higher-order splines and rapid initial time sampling will yield compartmental model parameter estimates that have smaller bias and larger uncertainty, compared to estimates obtained with lower-order splines and time sampling that is more uniform.

II. Methods

A. Direct Temporal B-Spline Model Estimation

Smooth time-activity curves for segmented volumes encompassing the projected field of view can be estimated directly from dynamic SPECT projection data as follows. This method can be applied to projection data acquired with the use of any collimator or orbit geometry, provided that the data yield a preliminary image reconstruction (e.g., from late time frames) that can be used to segment the activity distribution throughout the projected field of view.

The time-activity curve for segmented volume m is denoted by $A^m(t)$ and is modeled as a sum of temporal B-spline basis functions:

$$A^m(t) = \sum_{n=1}^{N} a_{mn} V^n(t), \tag{1}$$

where a_{mn} are model coefficients, $V^n(t)$ are the B-spline basis functions [12], and N is the number of basis functions. Splines with smaller support typically are used to model rapidly changing portions of curves, while splines with larger support are used to model slow changes (e.g., [13]).

Manuscript received December 2, 2002; revised September 4, 2003. This work was supported by the National Heart, Lung, and Blood Institute of the U.S. Department of Health and Human Services under grants R01-HL50663 and P01-HL25840 and by the Director, Office of Science, Office of Biological and Environmental Research, Medical Sciences Division of the U.S. Department of Energy under contract DE-AC03-76SF00098. This work was developed in part with the use of resources at the U.S. Department of Energy National Energy Research Scientific Computing (NERSC) Center.

The authors are with the Department of Nuclear Medicine and Functional Imaging, Lawrence Berkeley National Laboratory, University of California, Berkeley, CA 94720 USA (e-mail: bwreutter@lbl.gov).

The detected count rate at time t along ray i is modeled as

$$P_i(t) = \sum_{m=1}^{M} U_i^m(t) A^m(t) = \sum_{m=1}^{M}\sum_{n=1}^{N} a_{mn} U_i^m(t) V^n(t), \quad (2)$$

where $U_i^m(t)$ is the spatial projection, along ray i, of the indicator function for volume m and M is the number of segmented volumes encompassing the projected field of view. In practice, the spatial segmentation can be derived from static functional images obtained by summing late time frames of the dynamic SPECT study [3] and from registered anatomical images obtained from a transmission scan or X-ray computed tomography scan.

The model for the dynamic projection data is obtained by integrating (2) over L contiguous time intervals that span the data acquisition from time $t_0 = 0$ to time $t_L = T$:

$$p_{il} = \sum_{m=1}^{M}\sum_{n=1}^{N} a_{mn} \int_{t_{l-1}}^{t_l} U_i^m(\tau) V^n(\tau) d\tau. \quad (3)$$

If the time intervals are short enough so that each segmented volume projection function $U_i^m(t)$ is approximated well by a piecewise constant function with amplitude u_{il}^m during time interval $[t_{l-1}, t_l]$, then the model for the projection data can be simplified:

$$p_{il} = \sum_{m=1}^{M}\sum_{n=1}^{N} a_{mn} u_{il}^m v_l^n, \quad (4)$$

where v_l^n are the integrals $\int_{t_{l-1}}^{t_l} V^n(\tau)d\tau$ of the temporal B-spline basis functions.

The temporal spline model coefficients a_{mn} are estimated by minimizing the sum of squared differences between the measured and modeled projections:

$$\chi^2 = \sum_{i=1}^{I}\sum_{l=1}^{L} (p_{il}^* - p_{il})^2, \quad (5)$$

where p_{il}^* are the measured projections and I is the number of projection rays acquired simultaneously by the detector(s). For a periodic (e.g., multi-rotation circular) orbit, the spline model coefficients a_{mn}, their covariance matrix, and the global precision of the time-activity curve models can be estimated with the use of fast methods that take advantage of periodicity in the u_{il}^m factors [6], [10].

B. Nonlinear Compartmental Modeling

Directly estimated spline models yield smooth time-activity curves that can have a variety of shapes. In many cases the relationship between the time-activity curves for the blood pool and a tissue volume of interest is described accurately by a compartmental model. The compartmental model parameters have physiological meaning and can provide a quantitative measure of tissue perfusion [1]. It has been hypothesized that compartmental analysis may also be useful for assessing tissue viability [4].

For the one-compartment kinetic model (Fig. 1), the relationship between the blood input function, $B(t)$, and the activity

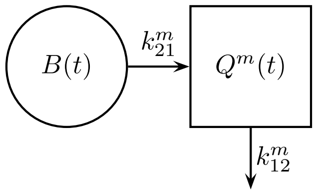

Fig. 1. Compartmental model for ^{99m}Tc-teboroxime in the myocardium.

in the tissue in volume m, $Q^m(t)$, is modeled to be

$$\frac{dQ^m(t)}{dt} = k_{21}^m B(t) - k_{12}^m Q^m(t), \quad (6)$$

where k_{21}^m is the uptake rate parameter and k_{12}^m is the washout rate parameter. For initial conditions of zero, the tissue activity is the convolution of the blood input function with a single decaying exponential:

$$Q^m(t) = k_{21}^m \int_0^t B(\tau) e^{-k_{12}^m (t-\tau)} d\tau = k_{21}^m C^m(t). \quad (7)$$

Total activity in volume m is given by $k_{21}^m C^m(t) + f_v^m B(t)$, where f_v^m is the fraction of vasculature in the volume.

The compartmental model parameters k_{21}^m, k_{12}^m, and f_v^m are estimated by minimizing the sum of squared differences between the spline and compartmental models:

$$\chi_m^2 = \sum_{l=1}^{L} \left\{ \sum_{n=1}^{N} \hat{a}_{mn} v_l^n - \int_{t_{l-1}}^{t_l} [k_{21}^m \hat{C}^m(\tau) + f_v^m \hat{B}(\tau)] d\tau \right\}^2, \quad (8)$$

where $\hat{a}_{mn}$ are values for spline model coefficients that minimize (5), $\sum_{n=1}^{N} \hat{a}_{mn} v_l^n$ is the integral of the temporal spline model for total activity in volume m during time interval $[t_{l-1}, t_l]$, $\hat{C}^m(\tau)$ is the convolution $\int_0^\tau \hat{B}(\tau') e^{-k_{12}^m(\tau-\tau')} d\tau'$, and $\hat{B}(\tau)$ is derived from the temporal spline model for activity in the blood pool.

III. Computer Simulations

We performed Monte Carlo simulations of realistic dynamic cardiac ^{99m}Tc-teboroxime patient studies acquired on a single-detector SPECT system. The goal was to determine how the polynomial order and initial time sampling of temporal B-spline basis functions affect the accuracy and precision of compartmental model parameters obtained from time-activity curves estimated directly from projection data. Effects of noise level in the projection data were also studied by simulating patient studies in which 20 million, 10 million, or 5 million total events were detected. The 10 million event level was comparable to that of an actual dynamic cardiac ^{99m}Tc-teboroxime patient study that we analyzed [3], after adjusting for differences in the number of detectors and collimator sensitivity.

A. Spatiotemporal Phantom

Simulated spatial distributions were obtained with the use of the Mathematical Cardiac Torso (MCAT) phantom [14]. The emission phantom (Fig. 2) was composed of 128 contiguous

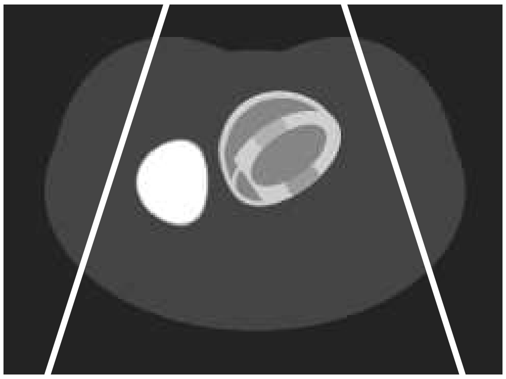

Fig. 2. Transverse cross section through MCAT emission phantom. White lines depict data truncation that results from use of cone beam collimators.

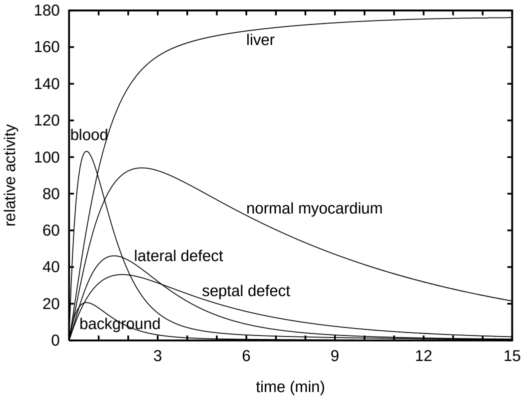

Fig. 3. Simulated ^{99m}Tc-teboroxime time-activity curves.

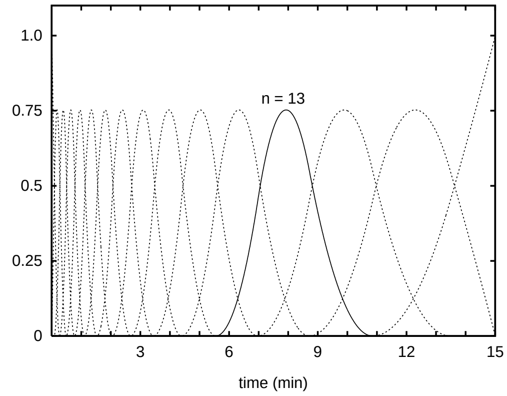

Fig. 4. Sixteen piecewise quadratic B-spline temporal basis functions that have an initial time segment length of 10 s. The thirteenth spline is shown as a solid curve.

1.75 mm-thick slices and contained $M = 6$ volumes of interest: the blood pool, three myocardial tissue volumes (normal myocardium, septal defect, and lateral defect), liver, and background tissue. The myocardial defects were located toward the inferior wall of the heart in transverse planes containing the liver, to make quantitation of activity in the defects challenging. Each volume was modeled to contain spatially uniform activity. Cardiac contraction and respiratory motion were not simulated.

The simulated time-activity curves for the six emission volumes are shown in Fig. 3. The time-activity curves for the three myocardial volumes of interest and the liver were generated by using the blood pool curve as the input to one-compartment models that have kinetics corresponding to those of ^{99m}Tc-teboroxime [15].

The simulated 15-min dynamic SPECT data acquisition consisted of one 360° circular rotation per minute and 120 projection angles per rotation. Projection data were obtained simultaneously along $I = 2048$ rays (64 transverse $\times$ 32 axial) during each of $L = 1800$ contiguous 0.5-s time intervals, to yield a total of about 3.7 million projection measurements. The projection bins were 7 mm $\times$ 7 mm at the detector, which was 30 cm from the center of the field of view. The detector was offset 1 cm from cone beam collimators that had a hole diameter of 2 mm and a length of 4 mm. The focal length of the collimators was 70 cm, which resulted in truncation of the data (Fig. 2). Projections were attenuated using the corresponding MCAT attenuation phantom. Attenuation and geometric point response were modeled using a ray-driven projector with line length weighting [16]. Scatter was not modeled.

B. Temporal B-spline Basis Sets

For each of 24 sets of temporal B-spline basis functions, time-activity curve models were estimated directly from 1000 realizations of data containing about 10 million total detected events with Poisson noise. Each set of basis functions consisted of $N = 16$ splines that spanned 15 time segments having geometrically increasing length (e.g., Fig. 4). The polynomial order and initial time sampling were varied systematically to study trade-offs between accuracy and precision of subsequent compartmental model parameter estimates. Piecewise cubic, quadratic, linear, or constant B-splines were used with initial time segment lengths of 2.5, 5, 10, 20, 40, or 60 s. The shorter initial time segment lengths provided a higher density of temporal spline basis functions at the beginning of the simulated acquisition, when activity concentrations were changing most rapidly (Fig. 3). The 60 s initial time segment length provided basis functions spaced uniformly in time. The cubic, quadratic, and linear B-splines allowed modeling of curves that were continuous through their second, first, and zeroth derivative, respectively.

Cubic or quadratic B-splines with initial time segment lengths of 2.5, 5, 10, or 20 s were also used to estimate time-activity curves directly from 1000 realizations of data containing either 5 million or 20 million total detected events with Poisson noise.

Given a temporal B-spline basis set and a noisy realization of projection data (e.g., Fig. 5), we calculated the 96 a_{mn} coefficients, their covariance matrix, and the global precision of the time-activity curve models in 34 s using a 194-MHz R10000-based SGI workstation and the fast methods presented in [6], [10]. Fig. 6 shows examples of spline models for time-activity curves estimated for the blood pool and the three myocardial volumes of interest, at the three different noise levels. Errors in amplitude estimates for adjacent temporal spline basis functions were negatively correlated and yielded excursions that alternated above and below the simulated time-

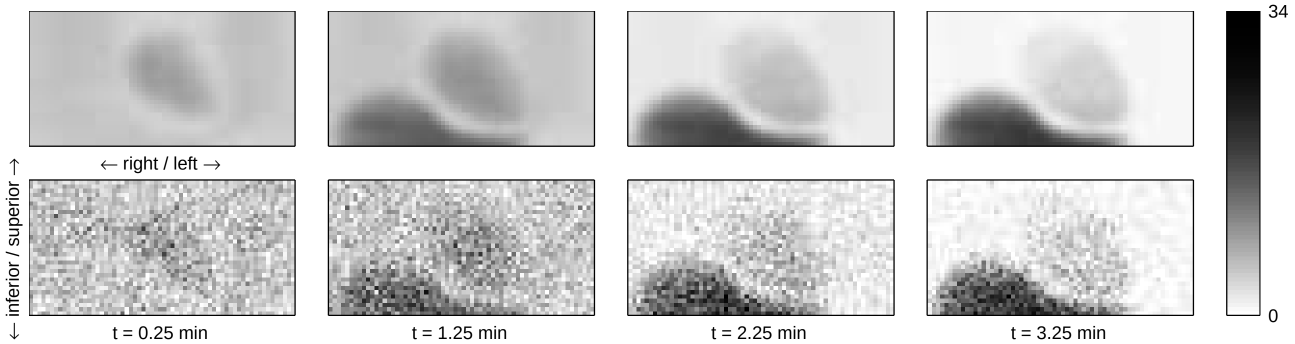

Fig. 5. Noiseless (upper) and noisy (lower) anterior projection data for the first four rotations of a simulated dynamic data acquisition in which 10 million total events are detected. Activity is seen first in the myocardial blood pool (structure in middle of field of view) and in the background tissue, followed by uptake in the myocardium (structure in middle of field of view) and liver (structure along bottom of field of view). Reduced accumulation of activity in the myocardial defects is difficult to detect visually, even in noiseless projections for the third and fourth rotations.

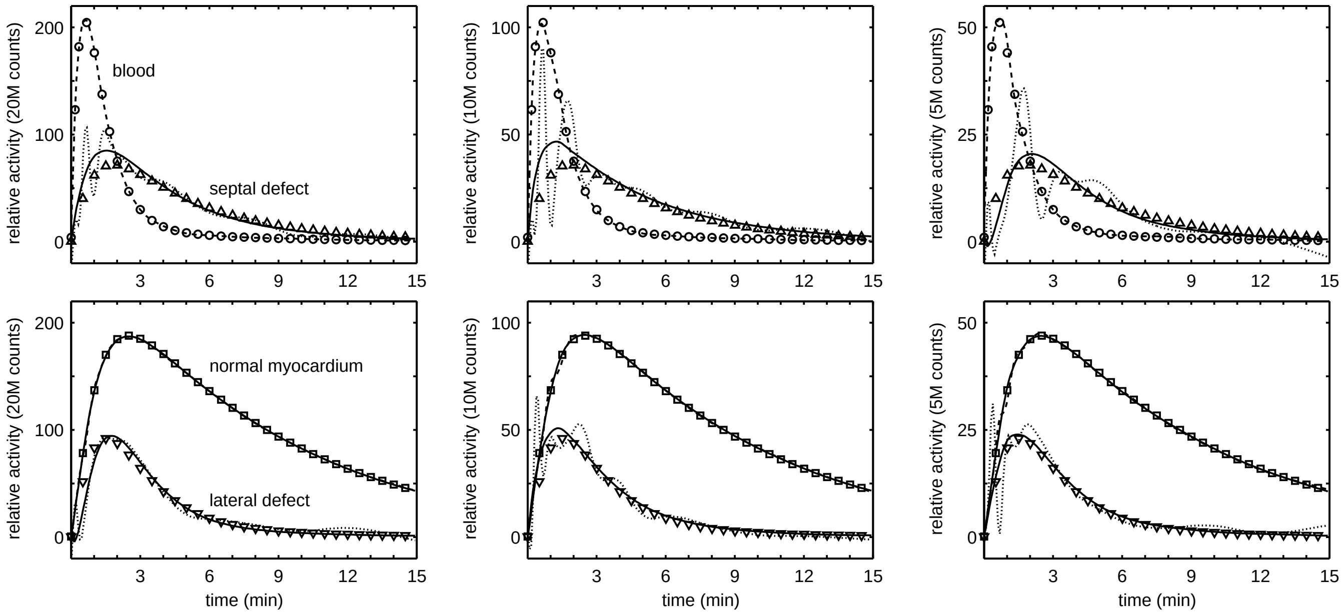

Fig. 6. Time-activity curve estimates for the blood pool and septal defect (upper) and for the normal myocardium and lateral defect (lower), for simulated noisy dynamic studies containing 20 million (left), 10 million (center), and 5 million (right) total detected events. Directly estimated spline time-activity curves are depicted by dashed lines for the blood pool and normal myocardium and by dotted lines for the defects. Solid lines depict curves for compartmental models estimated subsequently for the normal myocardium and defects. Samples of the simulated curves (Fig. 3) are shown as points.

activity curve, much like the noise in adjacent spatial voxels of a tomographic image reconstruction. The magnitudes of the excursions tended to decrease as the temporal supports of the spline basis functions increased, again analogous to noise seen in larger versus smaller spatial voxels.

C. Compartmental Model Estimates

Given spline time-activity curve models obtained from a noisy realization of projection data, we estimated compartmental model parameters in 18 s using the program RFIT [17]. Compartmental modeling provided additional temporal regularization that smoothed out excursions seen in early portions of the spline time-activity curves (Fig. 6). The relative accuracy and precision of the clinically relevant tissue uptake parameter k_{21} and tissue washout parameter k_{12} are shown in Figs. 7 and 8, respectively. Relative bias was calculated as the magnitude of the difference between the sample mean and the simulated value, normalized by the simulated value. The coefficient of variation was calculated by normalizing the sample standard deviation by the simulated value. For 10 million detected events, the use of cubic, quadratic, or linear splines and an initial time sampling of 20 s or less reduced uptake and washout parameter bias substantially without unduly increasing the coefficient of variation.

For the large volume of normal myocardium (250 cc), the relative bias of the sample means of the uptake and washout parameters did not exceed 0.3% at 10 million events, for cubic or quadratic splines and an initial time sampling of 20 s or less. The coefficient of variation of the parameters was about 1%.

The relative bias and coefficient of variation increased for the small (8.4 cc) defects that exhibited reduced uptake and accelerated washout. At 10 million events the maximum values of relative bias for the septal and lateral defects were about 5% and 16%, respectively, for cubic or quadratic splines and an

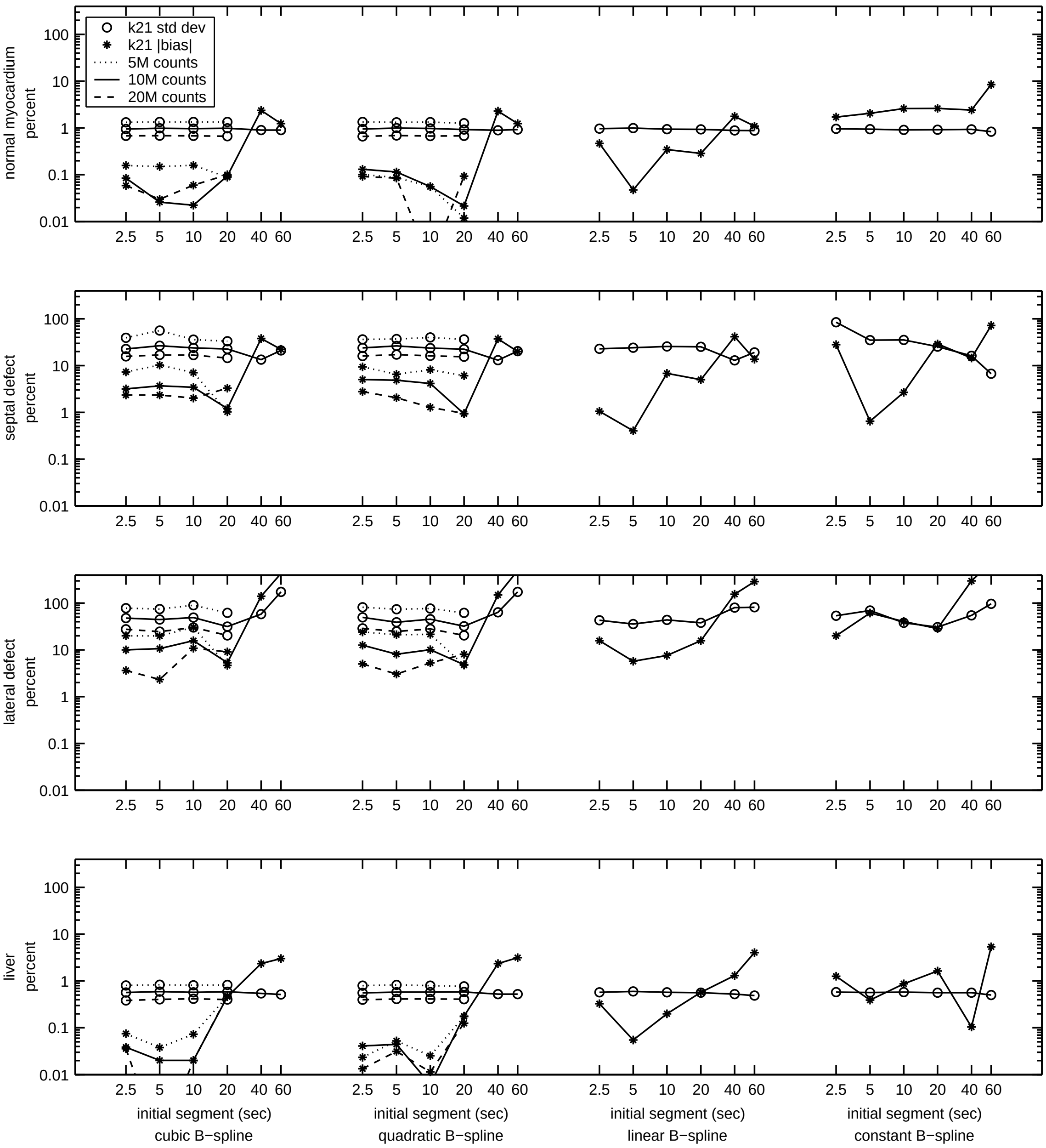

Fig. 7. Effects of temporal spline modeling on the tissue uptake parameter, k_{21}^{m}. The simulated values for normal myocardium, septal defect, lateral defect, and liver were 0.7, 0.3, 0.5, and 0.9 min^{-1}, respectively. The "$*$" symbols denote relative bias values observed for 1000 realizations of noisy projections. The "$\circ$" symbols denote the observed coefficients of variation. Dotted, solid, and dashed lines depict results for studies containing 5 million, 10 million, and 20 million total detected events, respectively.

initial time sampling of 20 s or less. Maximum values of the coefficient of variation were about 27% and 50%, respectively, for the septal and lateral defects. The increases were due to the relatively small size of the defects and the relatively small amplitude and narrow width of the peaks of their simulated time-activity curves. Nonetheless, these levels of accuracy and precision in the compartmental model parameters allowed the defects to be discriminated from the normal myocardium. As seen in Fig. 6, there was good contrast between the compartmental model time-activity curves for the defects and the normal myocardium.

For the large volume of liver (1100 cc) that exhibited the largest uptake, the relative bias and coefficient of variation of the uptake parameter did not exceed 0.5% and 0.6%, respectively, for 10 million events and cubic or quadratic splines and an initial time sampling of 20 s or less. Because the 500-min time constant for washout from the liver was extremely long compared to the 15-min duration of the simulated study (Fig. 3), the relative bias and coefficient of variation of the washout rate parameter increased to maximum values of about 3% and 21%, respectively, for cubic or quadratic splines and an initial time sampling of 20 s or less. The absolute bias and standard deviation were relatively small, however.

Changing the number of detected events by a factor of two had small absolute effects on the bias of the uptake and washout parameters for the normal myocardium and liver,

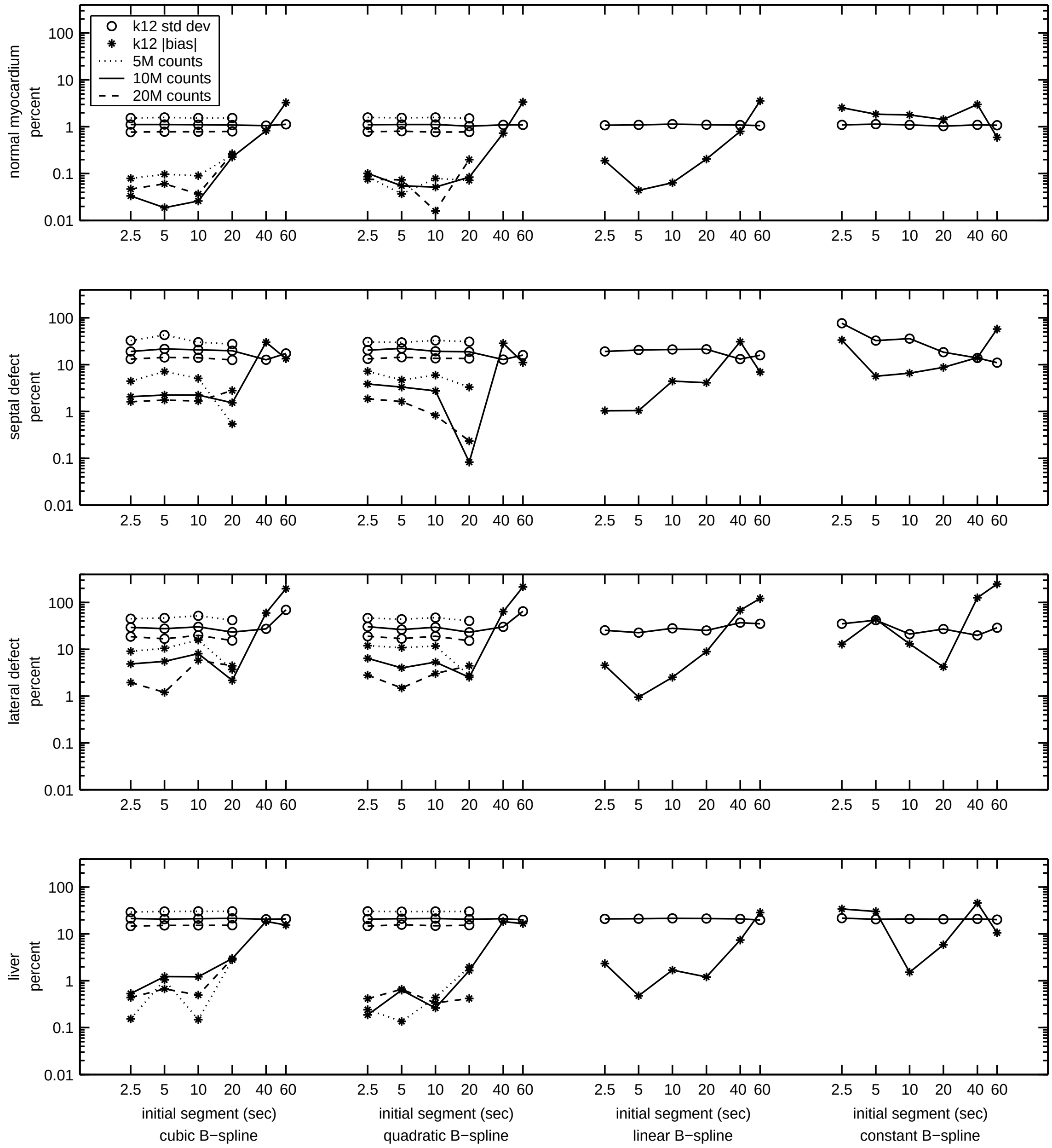

Fig. 8. Effects of temporal spline modeling on the tissue washout parameter, k_{12}^{m}. The simulated values for normal myocardium, septal defect, lateral defect, and liver were 0.15, 0.3, 0.6, and 0.002 min^{-1}, respectively. The "$*$" symbols denote relative bias values observed for 1000 realizations of noisy projections. The "$\circ$" symbols denote the observed coefficients of variation. Dotted, solid, and dashed lines depict results for studies containing 5 million, 10 million, and 20 million total detected events, respectively.

for cubic or quadratic splines and an initial time sampling of 20 s or less (Figs. 7 and 8). Maximum relative bias at 5 million or 20 million events did not exceed that observed at 10 million events. As expected, the coefficient of variation of the parameters increased by a factor of $1.4 \approx \sqrt{2}$ for 5 million events and decreased by a factor of 1.4 for 20 million events, compared to that observed at 10 million events.

Changing the number of detected events had a larger effect on the bias and variance of the uptake and washout parameters for the septal and lateral defects. At 5 million events the maximum values of relative bias for the septal and lateral defects increased to about 10% and 31%, respectively. At 20 million events the maximum values of relative bias decreased to about 3% and 11%, respectively, for the septal and lateral defects. The coefficient of variation of the parameters increased by a factor ranging between 1.5 and 1.8 for 5 million events and decreased by a factor ranging between 1.5 and 1.7 for 20 million events. Despite apparent nonlinearities in noise propagation for the defects, there was still good contrast between the compartmental model time-activity curves for the defects and the normal myocardium at 5 million events (Fig. 6).

IV. Discussion

The computer simulation results presented in Section III suggest that accurate and precise estimates of compartmental model parameters for relatively large tissue volumes can be obtained quickly from time-activity curves estimated directly from dynamic SPECT projection data. In addition, good contrast can be achieved between small myocardial defects and normal myocardium. Piecewise cubic or quadratic B-spline basis functions can model typical time-activity curves accurately and provide desired temporal regularization.

We have begun to study the effects of scatter modeling on directly estimated spline time-activity curves and subsequent compartmental model estimates [18]. We have also begun to implement methods for refining compartmental model estimates by jointly estimating the blood time-activity spline curve and tissue compartmental models directly from projection data [11]. Incorporation of the compartmental relationship between blood and tissue activities into the model for the projection data provides more temporal regularization than is provided by splines alone. For example, the use of splines as described in Section II-A introduces 16 parameters for each volume of interest and imposes no functional form on the relationship between the blood and tissue time-activity curves. By comparison, the use of one-compartment models introduces only three parameters for each tissue volume and constrains the tissue activity to be a convolution of the blood activity. This additional temporal regularization in the model for the projection data may improve the accuracy and precision of compartmental models for relatively small tissue volumes such as the myocardial defects simulated in Section III.

To improve the detail of spatial modeling, we plan to parameterize spatially nonuniform activity distributions within the segmented volumes. For example, activity within the segmented left ventricular myocardium could be modeled with the use of spherical harmonic basis functions.

Future work also includes dealing with patient and organ motion. For cardiac gated studies, individual gates can be segmented and volume projection factors (i.e., u_{il}^{m} factors) can be calculated for each gate. This strategy can also be used for respiratory gated studies and studies in which patient or organ motion is monitored or can be detected in the projection data [19]–[21]. For ungated studies, the segmented volume boundaries can be blurred to compensate for partial volume effects arising from cardiac contraction and respiratory motion.

Acknowledgment

The authors thank Dr. Benjamin Tsui at Johns Hopkins University for making the MCAT phantom available. The authors also thank the reviewers for their helpful comments and suggestions.

This work was supported by the National Heart, Lung, and Blood Institute of the U.S. Department of Health and Human Services under grants R01-HL50663 and P01-HL25840 and by the Director, Office of Science, Office of Biological and Environmental Research, Medical Sciences Division of the U.S. Department of Energy under contract DE-AC03-76SF00098.

This work was developed in part with the use of resources at the U.S. Department of Energy National Energy Research Scientific Computing (NERSC) Center.

References

[1] E. V. R. Di Bella, S. G. Ross, D. J. Kadrmas, H. S. Khare, P. E. Christian, S. McJames, and G. T. Gullberg, “Compartmental modeling of technetium-99m-labeled teboroxime with dynamic single-photon emission computed tomography: Comparison with static thallium-201 in a canine model,” *Invest. Radiol.*, vol. 36, no. 3, pp. 178–185, 2001.

[2] R. H. Huesman, B. W. Reutter, G. L. Zeng, and G. T. Gullberg, “Kinetic parameter estimation from SPECT cone-beam projection measurements,” *Phys. Med. Biol.*, vol. 43, no. 4, pp. 973–982, 1998.

[3] B. W. Reutter, G. T. Gullberg, and R. H. Huesman, “Kinetic parameter estimation from dynamic cardiac patient SPECT projection measurements,” in *Proc. 1998 IEEE Nuclear Science Symp. Medical Imaging Conf., Toronto, Ontario, Canada*, R. Sudharsanan, Ed., 1999, pp. 1953–1958.

[4] G. T. Gullberg, R. H. Huesman, S. G. Ross, E. V. R. Di Bella, G. L. Zeng, B. W. Reutter, P. E. Christian, and S. A. Foresti, “Dynamic cardiac single-photon emission computed tomography,” in *Nuclear Cardiology: State of the Art and Future Directions*, B. L. Zaret and G. A. Beller, Eds. St. Louis, MO: Mosby, 1999, ch. 11, pp. 137–187.

[5] A. Sitek, E. V. R. Di Bella, and G. T. Gullberg, “Reconstruction from slow rotation dynamic SPECT using a factor model,” in *Proc. 16th Int. Conf. Information Processing in Medical Imaging, Visegrád, Hungary*, A. Kuba, M. Šámal, and A. Todd-Pokropek, Eds., 1999, pp. 436–441.

[6] B. W. Reutter, G. T. Gullberg, and R. H. Huesman, “Direct least-squares estimation of spatiotemporal distributions from dynamic SPECT projections using a spatial segmentation and temporal B-splines,” *IEEE Trans. Med. Imag.*, vol. 19, no. 5, pp. 434–450, May 2000.

[7] T. Farncombe, A. Celler, C. Bever, D. Noll, J. Maeght, and R. Harrop, “The incorporation of organ uptake into dynamic spect (dSPECT) image reconstruction,” *IEEE Trans. Nucl. Sci.*, vol. 48, no. 1, pp. 3–9, Feb. 2001.

[8] D. J. Kadrmas and G. T. Gullberg, “4D maximum *a posteriori* reconstruction in dynamic SPECT using a compartmental model-based prior,” *Phys. Med. Biol.*, vol. 46, no. 5, pp. 1553–1574, 2001.

[9] J. S. Maltz, “Optimal time-activity basis selection for exponential spectral analysis: Application to the solution of large dynamic emission tomographic reconstruction problems,” *IEEE Trans. Nucl. Sci.*, vol. 48, no. 4, pp. 1452–1464, Aug. 2001.

[10] B. W. Reutter, R. H. Huesman, and G. T. Gullberg, “Effects of temporal modelling on the statistical uncertainty of spatiotemporal distributions estimated directly from dynamic SPECT projections,” *Phys. Med. Biol.*, vol. 47, no. 15, pp. 2673–2683, 2002.

[11] B. W. Reutter, G. T. Gullberg, and R. H. Huesman, “Fully 4-D direct joint estimation of compartmental models and blood input function from dynamic SPECT projections,” in *Proc. VIIth Int. Conf. Fully 3D Reconstruction in Radiology and Nuclear Medicine, Saint Malo, France*, Y. Bizais, Ed., 2003, pp. Mo–PM3–1/1–4.

[12] R. H. Bartels, J. C. Beatty, and B. A. Barsky, *An Introduction to Splines for Use in Computer Graphics and Geometric Modeling*. Los Altos, CA: Morgan Kaufmann, 1987.

[13] T. E. Nichols, J. Qi, E. Asma, and R. M. Leahy, “Spatiotemporal reconstruction of list-mode PET data,” *IEEE Trans. Med. Imag.*, vol. 21, no. 4, pp. 396–404, Apr. 2000.

[14] B. M. W. Tsui, J. A. Terry, and G. T. Gullberg, “Evaluation of cardiac cone-beam single photon emission computed tomography using observer performance experiments and receiver operating characteristic analysis,” *Invest. Radiol.*, vol. 28, no. 12, pp. 1101–1112, 1993.

[15] R. K. Narra, T. Feld, and A. D. Nunn, “Absorbed radiation dose to humans from technetium-99m-teboroxime,” *J. Nucl. Med.*, vol. 33, no. 1, pp. 88–93, 1992.

[16] G. L. Zeng, G. T. Gullberg, B. M. W. Tsui, and J. A. Terry, “Three-dimensional iterative reconstruction algorithms with attenuation and geometric point response correction,” *IEEE Trans. Nucl. Sci.*, vol. 38, no. 2, pp. 693–702, Apr. 1991.

[17] R. H. Huesman, B. L. Knittel, B. M. Mazoyer, P. G. Coxson, E. M. Salmeron, G. J. Klein, B. W. Reutter, and T. F. Budinger, “Notes on RFIT: A program for fitting compartmental models to region-of-interest dynamic emission tomography data,” Lawrence Berkeley National Laboratory, Tech. Rep. LBL-37621, 1995.

[18] B. W. Reutter, G. T. Gullberg, and R. H. Huesman, “Effects of scatter modeling on time-activity curves estimated directly from dynamic SPECT projections,” in *Proc. 2003 IEEE Nuclear Science Symp. Medical Imaging Conf., Portland, Oregon, USA*, S. Metzler, Ed., 2004, in press.

[19] G. Germano, T. Chua, P. B. Kavanagh, H. Kiat, and D. S. Berman, “Detection and correction of patient motion in dynamic and static myocardial SPECT using a multi-detector camera,” *J. Nucl. Med.*, vol. 34, no. 8, pp. 1349–1355, 1993.

[20] G. J. Klein, B. W. Reutter, M. H. Ho, J. H. Reed, and R. H. Huesman, “Real-time system for respiratory-cardiac gating in positron tomography,” *IEEE Trans. Nucl. Sci.*, vol. 45, no. 4, pp. 2139–2143, Aug. 1998.

[21] G. J. Klein, B. W. Reutter, E. H. Botvinick, T. F. Budinger, and R. H. Huesman, “Fine-scale motion detection using intrinsic list mode PET information,” in *Proc. 2001 IEEE Workshop Mathematical Methods in Biomedical Image Analysis, Kauai, Hawaii, USA*, L. Staib, Ed., 2001, pp. 71–78.

Disclaimer